DR. LAURA NICOLAOU (Orcid ID : 0000-0003-2539-9620)
DR. KIRSTEN KOEHLER (Orcid ID : 0000-0002-0516-6945)
DR. WILLIAM CHECKLEY (Orcid ID : 0000-0003-1106-8812)

Article type : Original Article

Size Distribution and Lung-Deposited Doses of Particulate Matter From Household Exposure to Biomass Smoke

Running title: Biomass smoke particle sizes and lung deposition

Laura Nicolaou[1,2,*], Magdalena Fandiño-Del-Rio[2,3], Kirsten Koehler[3], William Checkley[1,2], CHAP trial Investigators

1. Division of Pulmonary and Critical Care, School of Medicine, Johns Hopkins University, Baltimore, MD 21287, USA
2. Center for Global Non-Communicable Disease Research and Training, Johns Hopkins University, Baltimore, MD 21287, USA
3. Department of Environmental Health and Engineering, Bloomberg School of Public Health, Johns Hopkins University, Baltimore, MD, 21205, USA

[*]**Corresponding author:** Laura Nicolaou PhD. E-mail: l.nicolaou@jhu.edu

Cardiopulmonary outcomes and Household Air Pollution (CHAP) trial Investigators listed in Appendix.

Acknowledgments

The parent study reported in this publication was supported by the United States National Institutes of Health through the following Institutes and Centres: Fogarty International Center, National Institute of Environmental Health Sciences, National Cancer Institute, and Centers for Disease Control under award number U01TW010107 (MPIs: Checkley, Gonzales, Naeher, Steenland). The trial was

additionally supported in part by the Clean Cooking Alliance of the United Nations Foundation UNF-16-810 (PI: Checkley), and Ms Fandiño-Del-Rio was further supported by the Global Environmental and Occupational Health (GEOHealth), Fogarty International Center. Dr Nicolaou and our Global Non-Communicable Disease Research and Training field centre in Puno, Peru, also received generous support from Mr. William and Bonnie Clarke III.

Conflict of interest: We declare no competing interests.

Abstract

Exposure to high concentrations of particulate matter (PM) is associated with a number of adverse health effects. However, it is unclear which aspects of PM are most hazardous, and a better understanding of particle sizes and personal exposure is needed. We characterized particle size distribution (PSD) from biomass-related pollution and assessed total and regional lung-deposited doses using multiple-path deposition modeling. Gravimetric measurements of kitchen and personal $PM_{2.5}$ (< 2.5 μm in size) exposures were collected in 180 households in rural Puno, Peru. Direct-reading measurements of number concentrations were collected in a subset of 20 kitchens for particles 0.3–25 μm, and the continuous PSD was derived using a nonlinear least-squares method. Mean daily $PM_{2.5}$ kitchen concentration and personal exposure was 1205±942 $\mu g/m^3$ and 115±167 $\mu g/m^3$ respectively, and the mean mass concentration consisted of a primary accumulation mode at 0.21 μm and a secondary coarse mode at 3.17 μm. Mean daily lung-deposited surface area (LDSA) and LDSA during cooking were 1009.6±1469.8 $\mu m^2/cm^3$ and 10,552.5±8261.6 $\mu m^2/cm^3$, respectively. This study presents unique data regarding lung deposition of biomass smoke that could serve as a reference for future studies, and provides a novel, more biologically-relevant metric for exposure-response analysis compared to traditional size-based metrics.

Keywords: Biomass fuels, Cookstoves, Environmental exposure, Indoor air pollution, Particle size distribution, Lung deposition

Practical implications

Biomass fuels are burned for domestic use by an estimated 3 billion people worldwide, and emit high concentrations of harmful pollutants including particulate matter (PM), when used in open fires and inefficient cookstoves. While studies have measured area concentrations and personal exposures to PM from biomass burning, few have examined the particle size distribution, which plays a critical role on the inhaled dose, and assessments of the lung-deposited dose, which is a more biologically-relevant exposure metric, are lacking. Our work provides novel data on PM deposition in the lungs from biomass burning, and demonstrates the potential use of lung deposition models for exposure risk assessment. Regional deposition estimates reveal the areas of the lung receiving the highest cumulative doses, which could indicate the sites most prone to inflammation and disease initiation, and the lung-deposited dose could be used to develop improved dose-response curves.

1 Introduction

Approximately 40% of the population, the majority from low- and middle-income countries, relies on coal and biomass as their primary source of domestic energy [1]. The low combustion efficiency of these fuels, often coupled with a lack of ventilation and poor cookstove design, leads to high concentration levels of pollutants that are damaging to health. These include particulate matter (PM), carbon monoxide, nitrous oxides and black carbon. Continued exposure to these pollutants has been associated with an increased risk of chronic obstructive pulmonary disease (COPD), acute respiratory infections, and cardiovascular disease [2]. Evidence is also emerging that exposure to biomass smoke increases the risk of other conditions, such as tuberculosis, asthma, lung cancer, low birth weight, and perinatal mortality [1,3]. According to the World Health Organization (WHO), household air pollution (HAP) is the fourth leading cause of death worldwide and was responsible for 3.8 million premature deaths in 2016 [4]. Women and young children, who are most heavily exposed, bear the brunt of this disease burden [5].

Particles with diameters of 10 μm or smaller (PM_{10}), and particularly fine particles 2.5 μm or smaller in diameter ($PM_{2.5}$), pose a health hazard as they can penetrate deep into the lungs. Long-term exposure to $PM_{2.5}$ above a mean concentration of 10 $\mu g/m^3$ has been shown to increase the risk of cardiopulmonary and lung cancer mortality [6]. Based on this criterion, the WHO defined a guideline value for annual mean $PM_{2.5}$ of 10 $\mu g/m^3$. Besides this guideline value, three interim targets (IT) were also set at progressively lower concentrations, with the least-stringent interim target of 35 $\mu g/m^3$ (IT-1). In kitchens using biomass cookstoves, however, mean daily $PM_{2.5}$ concentrations are typically in the range of 1000 to 3000 $\mu g/m^3$, with concentrations of 8000 $\mu g/m^3$ or higher possible during periods of cooking [7-9].

In addition to kitchen concentrations of PM, studies have also started measuring personal exposures to obtain more accurate measures of the concentrations to which people are exposed [10-12]. While personal exposure measures are more representative of the inhaled PM concentrations, not all particles that are inhaled deposit in the lungs. Furthermore, personal exposure concentrations may not correlate with health effects if the risk is associated only with particles that reach the intrathoracic airways or that penetrate beyond the ciliated airways into the respiratory zone. The deposited doses in different regions of the lung are therefore a more biologically-relevant metric to associate with health

outcomes compared to personal exposure alone. To the best of our knowledge, this has not been investigated for PM emitted from biomass cookstoves.

To estimate lung deposition, knowledge of the PM particle size distribution (PSD) is required, as particle size plays a major role on both the amount and location of deposition in the lungs [13,14]. Few studies have examined the PSD of particulate matter generated by biomass-burning cookstoves, and the results have shown a wide variation in PSD due to differing combustion conditions and measurement technologies [15]. Using an aerodynamic particle sizer (APS), Park and Lee [7] measured PSD in 23 houses with wood-burning stoves in Costa Rica, and found that all houses had a PSD of either one or two peaks at around 0.7 and 2.5 μm aerodynamic diameters, with the majority of homes displaying two peaks. On the other hand, results from a study performed in a laboratory hood chamber using 10 different biomass materials revealed that, regardless of biomass type, the shape of the normalized mass size distribution displayed a unimodal distribution with a peak between either 0.32 and 0.55 μm or 0.55 and 1.00 μm [16]. Armendáriz-Arnez et al. [11] collected PM samples in 11 homes using open fires in Tanaco, Mexico, using a 4-stage cascade impactor with particle size bins of < 0.25, 0.25–0.5, 0.5–1.0, 1.0–2.5 and > 2.5 μm. The smallest (< 0.25 μm) and largest particle size fraction (> 2.5 μm) were found to contribute the largest and second largest fraction of particulate mass concentration, respectively. The variability in the results highlights the importance of characterizing PSD in different settings.

In this study, we sought to assess the PSD and lung-deposited dose of PM emissions from biomass cookstoves in the Peruvian Andes. To this end, we collected gravimetric samples of kitchen $PM_{2.5}$ concentrations and personal $PM_{2.5}$ exposures in 180 households in rural Puno, Peru, and measured number concentrations in six size bins between 0.3 and 25 μm in diameter, using an optical particle counter (OPC) in a subset of 20 kitchens. We examined the average PM variation throughout the day and computed the mean daily PSD. We then determined deposition fractions in ten whole-lung models representative of the respiratory airways of adult Andean women, to account for inter-subject variability, and estimated mean daily total and regional lung-deposited doses. To the best of our knowledge this is the first study to provide direct-reading size-resolved PM measurements and to examine lung-deposited doses and regional airway deposition of PM from biomass cookstoves.

2 Methods

2.1 Parent study and research location

Primary data collection was conducted in rural communities of the southern Peruvian province of Puno, which is located at an altitude of 3825 meters above sea level and has a population of 219,494 inhabitants [17]. The parent study is a randomized, controlled field intervention trial of liquified petroleum gas (LPG) stoves and fuel distribution in which 180 female participants were enrolled and followed for 2 years. Participants lived in rural communities where traditional, open-fire stoves with biomass fuels (i.e., wood, animal dung, and crop residue) are used for cooking. To be eligible for the trial, women had to be aged 25–64 years, be the primary cook, use biomass fuels daily for cooking, and have a cooking area separate from their sleeping area. One woman per household was enrolled, and HAP exposure assessments and longitudinal measurements of cardiovascular and pulmonary outcomes were performed over a two-year period. The protocol of this trial is described in detail elsewhere [18].

All participants provided written informed consent to take part in the study. The trial was approved by the Institutional Review Boards of A.B. PRISMA (CE2402.16) and Universidad Peruana Cayetano Heredia (66780) in Lima, Peru, and by the Johns Hopkins Bloomberg School of Public Health (00007128) in Baltimore, USA. The trial is registered in ClinicalTrials.gov (identifier NCT02994680).

2.2 Exposure assessment

Personal exposure and kitchen concentrations of $PM_{2.5}$ were measured over a 48-hour period with ECM monitors (RTI Inc., Research Triangle Park, NC, USA) at each exposure assessment visit of the parent study. Here, we use data from the baseline visit in which all 180 participants used their traditional biomass cookstoves for cooking. The ECM collects $PM_{2.5}$ on a 15-mm diameter filter using a 0.3 L/min pump. We used Teflon filters with a 2-µm membrane (Measurement Technology Laboratories LLC, Minneapolis, MN, USA), and calibrated the volumetric flowrate of the ECM pumps daily with a TSI 4100 flowmeter (TSI Incorporated, 500 Cardigan Road, Shoreview, MN, USA). Filter samples were analyzed gravimetrically. For kitchen concentration measurements, the ECMs were placed at a distance of approximately 1.5 m from the ground and 1.0 m from the cookstove. Kitchen samples included 10% blanks and 10% duplicates, and all concentrations were

blank-corrected. For personal exposure sampling, the ECM was worn by the participants near the breathing zone in the pocket of an apron provided to them. Participants were asked to wear the aprons during awake hours and place them near their beds when sleeping over the 48-hour sampling period.

In a subset of 20 households using traditional biomass cookstoves, we measured number concentrations of particles with the AeroTrak 9306-V2 particle counter (TSI Incorporated, Shoreview, MN, USA). The AeroTrak 9306-V2 is a lightweight handheld OPC, which operates at a flow rate of 2.83 L/min and simultaneously counts particles in 6 user-adjustable bin sizes from 0.3 to 25 μm. We set the bins to the following particle size ranges: 0.3–0.5 μm, 0.5–0.7 μm, 0.7–1.0 μm, 1.0–1.5 μm, 1.5–2.5 μm, and > 2.5 μm. Due to high concentrations of PM exceeding the concentration limits of the device (2.1×10^8 m^{-3}) during cooking events, we employed an HHAD aerosol dilutor (Millholland & Associates, Holly Springs, NC, USA) calibrated at a dilution factor of 100:1. The particle counter was collocated with the ECM monitor in the kitchens, and typically installed before or at the start of the main morning cooking event. One-minute samples were collected every minute, over 24 hours where external battery life allowed and 12 hours at minimum.

2.3 Lung deposition modeling

To determine the lung-deposited dose and regional deposition fractions of inhaled PM, we adopted the multiple-path deposition model developed by Anjilvel and Asgharian [19] on ten asymmetric stochastic airway geometries [20]. These bronchial tree geometries are constructed from the morphometric data measured at the Lovelace Respiratory Research Institute [21] and statistical distributions of length, diameter, branching angle, and gravity angle [22]. Each airway tube is based on a single selection from the individual parameter distributions. The constructed geometry therefore represents the bronchial tree of an individual rather than a population-averaged lung [20].

The ten asymmetric, structurally different airway trees were adopted to account for inter-subject variability, which has been shown to have a significant effect on particle deposition in the lungs [23-26]. These geometries vary in total number of airways, spanning the 1st through 99th percentile in size for adult human lungs. Due to a lack of sufficient airway measurements beyond the terminal bronchioles, alveolar regions from the five-lobe typical-path model of Yeh and Schum [27] are attached to the end of each terminal bronchiole to construct the complete lung geometry. Since the geometries have a different number of terminal airways, and therefore different number of alveolar

regions, the dimensions of the alveolar airways are adjusted such that the total alveolar volume is the same across all geometries [20]. Within each airway of the complete lung geometry, deposition is calculated using theoretically-derived efficiencies for deposition by diffusion, sedimentation, and impaction within the airway or airway bifurcation. Additional information on the respiratory system and deposition in the lungs is provided in Supporting Information section S1.1 and Figure S1.

Lung capacity and breathing parameters were set based on values found in the literature for adult Andean women where available, and adult Caucasian women otherwise. Functional residual capacity (FRC) was set to 2600 ml, based on the mean FRC measured in 192 adult non-pregnant Andean women [28], and upper respiratory tract volume was 50 ml, which is representative of adult Caucasian women [29]. We adopted a breathing frequency of 17 breaths per minute and a tidal volume (V_T) of 700 ml, corresponding to mean ventilatory characteristics of Aymara high-altitude adult women during relaxed nose breathing [30]. During respiration, equal inspiration and expiration times without pause were assumed, and the airways were assumed to expand and contract uniformly [20,31]. Particle deposition was computed at FRC + V_T/2, corresponding to an airway size midway between lung volume at rest and maximum inhalation. The gravimetric-corrected average mean daily PSD, derived from the kitchen area exposure measurements, was used as the inhaled mass. Details on how the continuous PSD model was computed from the discrete OPC data are provided in Supporting Information section S1.2. Based on this inhaled dose, regional, lobar, and per-generation depositions of particles were then calculated in the ten asymmetric lung models and mean daily lung-deposited doses were estimated.

Besides deposited mass, studies are increasingly showing that particle surface-related chemistry and, therefore, deposited surface area (DSA) is a relevant parameter to consider when determining the harmfulness of particulate matter [32, 33]. The lung-deposited surface area (LDSA) concentration, calculated assuming the particles are spheres and reported in $\mu m^2/cm^3$, is given by:

$$\text{LDSA concentration} = \frac{\sum_{i=1}^{n_{dep}} \pi \, {d_{p_i}}^2}{V_T},$$

where n_{dep} represents the number of deposited particles over one breath, and d_{p_i} (μm) is the diameter of the *i*th particle. The mean daily LDSA dose can be calculated from:

$$\text{daily LDSA} = 1440 f \sum_{i=1}^{n_{dep}} \pi \, {d_{p_i}}^2,$$

where f is the breathing frequency (breaths/min).

3 Results

3.1 Particulate matter concentrations and particle size distribution

Personal exposures and kitchen concentrations of $PM_{2.5}$ obtained from the 48-hour time-weighted gravimetric measurements are shown in Figure 1. Mean ± standard deviation (SD) daily personal exposure, μ_P, and kitchen concentration, μ_K, are 115.3 ± 166.9 μg/m^3 and 1205.0 ± 941.5 μg/m^3, respectively. These values substantially exceed the WHO's interim air quality target IT-1 of 35 μg/m^3. The corresponding median and interquartile ranges are 72.1 (39.4–130.3) μg/m^3 and 982.1 (422.3–1823.6) μg/m^3, respectively. The higher means than medians indicate the existence of extreme values on the right, which can also be observed in the box plots (Figure 1b). As is characteristic of lognormal distributions, both personal exposures and kitchen concentrations are positively skewed and heavy tailed, with adjusted Fisher-Pearson coefficients of 5.5 and 0.9, and kurtoses of 42.1 and 3.4 for personal and kitchen concentrations, respectively.

PM number concentrations throughout the day, averaged in two-hour intervals, are shown in Figure 2 for particles between 0.3 and 2.5 μm in diameter, in every sampled kitchen. Number concentrations range between 10^3 and 10^{11} m^{-3} depending on particle size, time of day, and household. In general, a decrease in number concentrations with increasing particle size is observed across all households and time intervals. High PM concentrations are seen during typical cooking times, primarily between 6 and 8 a.m. in most kitchens, with some households also showing high concentrations later in the day, corresponding to additional cooking events around midday and in the evening.

In Figure 3, we display the number-weighted and mass-weighted mean daily PSDs averaged across all sampled households. As in Figure 2, a significant decrease in number concentrations is observed with increasing particle size. The mass concentration shows a primary peak at the smallest particle size bin (0.3–0.5 μm), and a secondary peak for particles > 2.5 μm, which confirms the suitability of a bimodal distribution with an accumulation and a coarse mode to fit the data. The continuous PSD obtained via least-squares optimization is plotted over the discrete data in Figure 3b. The primary

mode in the accumulation regime has a geometric mean diameter, $d_{ga} = 0.21$ μm and a geometric standard deviation, $\sigma_{ga} = 1.50$, and contains 77.6% of the total mass. The secondary mode in the coarse regime has $d_{gc} = 3.17$ μm and $\sigma_{gc} = 2.95$.

From our PSD model, the estimated mean daily $PM_{2.5}$ kitchen concentration is 706 μg/m^3. Taking the ratio of mean daily $PM_{2.5}$ from the gravimetric measurements (1205 μg/m^3) to the OPC-derived mean value we obtain a correction factor of 1.71, which we use to calibrate the direct-reading mass concentrations. Mean daily total and PM_{10} kitchen concentrations, obtained from the gravimetric-corrected PSD, are 1386 μg/m^3 and 1343 μg/m^3, respectively. Figure 4 shows the mean variation in gravimetric-corrected PM mass concentrations and mass fractions throughout the day, time-averaged in 10-minute intervals, across all available one-minute samples at a given time of the day from the 20 sampled kitchens. Although the frequency and timing of cooking was variable across households, the results show that cooking was generally performed twice per day, with a main cooking event in the early morning and a shorter event in the evening. An additional short cooking event around midday was also observed in a few households, evident from the mass concentration peak around 1 p.m., which is lower in magnitude compared to the morning and evening peaks. A large variability in both the total concentration as well as the fraction of different particle sizes is observed throughout the day. During cooking times, the smallest particles (0.3–0.5 μm) make up the largest portion of the measured mass concentration, whereas during non-cooking periods, kitchen PM consists primarily of large particles above 2.5 μm, which are likely mostly dust.

To assess the variability in mass fractions and the suitability of our PSD model (Figure 3b), we computed the mass-weighted mean PSDs during cooking and non-cooking periods (Figure S3). The results show that the PSDs during cooking and non-cooking times are drastically different. However, since concentrations during cooking are two to three orders of magnitude higher, the PSD during non-cooking periods has a minor effect on the mean daily PSD. The mean daily PSD (Figure 3b) is therefore qualitatively similar to the PSD during cooking (Figure S3a), which indicates the suitability of our PSD model since exposures are driven by cooking events.

3.2 Lung deposited dose and regional deposition fractions

Using the gravimetric-corrected mean daily PSD as the inhaled mass, we modeled PM deposition in ten stochastic lung geometries, representative of the respiratory airways of adult Andean women. The lobar volumes of the lung geometries and their volumes by generation number are shown in Figures S4a and b, respectively. The variability among geometries is evident, with maximum differences in lobar volumes varying between 96.3% in the LU lobe and 151.9% in the RL lobe (Figure S4a). The volume-per-generation plot further reveals that differences in geometry at the local level can be substantial, with volumes at a given airway generation varying by as much as an order of magnitude (Figure S4b). We expect this geometric variation to consequently result in inter-subject variability in the total and regional PM deposition.

The total and regional deposition fractions in the extrathoracic airways (ETA), tracheobronchial (TB) and pulmonary regions of the lung, stratified by particle size mode (accumulation and coarse particle modes), are shown in Figure 5a. Total deposition is 33.0 ± 0.75% of the inhaled mass, with 14.9 ± 0.76% depositing in the intrathoracic airways. Only 14.4% of the coarse mode mass deposits in the lower respiratory tract. On the other hand, 77.1% of the mass in the accumulation mode clears the nose and throat and deposits in the intrathoracic airways, with 59.7% of this mass reaching the acinar region.

Deposition fraction by lobe is plotted in Figure 5b. A substantial variability exists across lung geometries, particularly in the right lung where deposited fractions vary by as much as a factor of 3.5, 7.3 and 7.1 in the right upper (RU), middle (RM) and lower (RL) lobes, respectively. On average, the left and right lungs receive 6.2% and 7.5% of the inhaled mass, respectively. The left lower (LL) and right upper (RU) lobes, with the largest volumes on average (Figure S4a), receive the highest fraction of mass, while the right middle (RM) lobe, which has the lowest lobar volume, has the lowest deposition fraction.

Deposited mass (DM) and deposited mass per tissue surface area (DM/TSA), also defined as the tissue dose, are plotted by generation number in Figures 6a and b, respectively. Two peaks in DM are observed: a primary one in the pulmonary region, with maximum deposition occurring between generations 18 and 22, and a secondary one in the upper bronchial airways, between generations 3 and 5. The accumulation mode particles, which constitute the bulk of the DM, deposit primarily in the

pulmonary region with peak DM over twice as high as in the upper bronchi, while coarse mode particles display a more even distribution between the two peaks. Notable differences in the deposited dose are observed across subjects, both in the upper bronchial airways and the acinar region. Normalizing by unit tissue surface area, we observe that the lobar and segmental bronchi (generations 3 and 4) receive the highest tissue doses (Figure 6b).

The deposited surface area (DSA) and DSA per tissue surface area (DSA/TSA) are shown in Figures 6c and d, respectively. DSA is shown to follow a similar trend to DM, with the bulk of the inhaled dose delivered to the pulmonary region (Figure 6c), and peak tissue doses in the lobar and segmental bronchi (Figure 6d). Across all airway generations, total DSA also consists of similar fractions of accumulation and coarse mode particles as total DM, which suggests that for this PSD, both metrics would be similar predictors of PM toxicity.

Since a portion of the accumulation mode lies outside the OPC's measurement limits, we performed a sensitivity analysis on our PSD model parameters to assess the effect of PSD uncertainty on lung deposition. The results of this analysis can be found in Supporting Information section S2.3.

Upper bound estimates of the daily lung-deposited mass (LDM) and daily lung-deposited surface area (LDSA), taking into account both geometric variability across the ten airway models and between-house variability across the 180 kitchen concentrations, are 7847.4 ± 6135.8 μg/day, and 1808.3 ± 1415.7 cm^2/day, respectively. Typically, however, the women do not remain in the kitchen for the entire cooking duration. Using the personal exposure concentrations instead, we can obtain more realistic estimates of the daily lung-deposited doses, assuming that the majority of personal PM exposure occurs in the kitchen. Table 1 summarizes the daily deposited doses in the different regions of the lungs and in the five lobes, based on mean ± SD deposition fractions across the ten airway models and mean ± SD personal exposure concentrations. The estimated mean daily LDM and LDSA are 750.8 ± 1092.2 μg/day and 173.0 ± 251.9 cm^2/day, respectively, with 339.0 ± 494.0 μg/day and 141.6 ± 206.2 cm^2/day depositing in the intrathoracic airways. This corresponds to mean daily LDM and LDSA concentrations of 43.8 ± 63.7 $\mu g/m^3$ and 1009.5 ±1469.8 $\mu m^2/cm^3$, with 19.8 ± 28.8 $\mu g/m^3$ and 826.2 ± 1203.6 $\mu m^2/cm^3$ depositing in the intrathoracic airways.

4 Discussion

Gravimetric measurements of kitchen and personal $PM_{2.5}$ exposures were collected in 180 households cooking with biomass cookstoves in rural Puno, Peru. Additionally, size-resolved number concentrations of particles between 0.3 and 25 μm in diameter were measured in a subset of 20 households to model the PSD of PM generated by biomass combustion, which has been assessed in only a handful of studies so far. Although the generalizability of our results is limited by the small sample size, PM concentration levels were in the range of those reported in the literature [7,8,11] and our PSD was consistent with distributions of smoke particles generated during biomass burning [34,35]. Another unique aspect of our study was the assessment of PM deposition in the lungs, which to the best of our knowledge has not been examined before for biomass cookstoves, and could provide a more relevant metric for association with health outcomes compared to personal exposure alone. Future work will be conducted to examine the differences in lung deposition between different types of biomass fuel and different stages in the combustion process, and to assess the effect of PSD variability.

Our results showed that cooking was generally performed twice a day in the sampled households, with a main cooking event in the early morning and a shorter event in the evening. A large variation in total PM concentrations, as well as particle size fractions, were observed throughout the day. Number concentrations ranged between 10^3 and 10^{11} m^{-3}, with a decrease in concentration with increasing particle size. The mass concentration displayed a bimodal lognormal distribution with a primary mode in the accumulation regime (GMD = 0.21 μm, GSD= 1.50) containing 78% of the total mass, and a secondary coarse mode (GMD = 3.17 μm, GSD= 2.95). Mean daily $PM_{2.5}$ kitchen concentration was 1205.0 ± 941.5 μg/m^3 and mean daily personal exposure was 115.3 ± 166.9 μg/m^3, exceeding WHO guidelines by an order of magnitude. While it is difficult to compare these values to other concentrations in the literature due to differences in sample durations, measurement techniques, fuel types and household characteristics among other factors, studies in other settings have reported comparable concentrations in households using open-fire biomass cookstoves, with kitchen area $PM_{2.5}$ between 257 μg/m^3 and 2740 μg/m^3 [8, 11, 36, 37], and personal exposures between 80 μg/m^3 and 202 μg/m^3 [10-12, 38]. A study conducted in two rural indigenous communities in the Bolivian Andes

[39], a similar study area and population to ours, reported a mean kitchen PM_{10} concentration of 1830 $\mu g/m^3$, which is in close agreement to our estimated mean kitchen PM_{10} of 1343 $\mu g/m^3$.

Mean total deposition across ten stochastic lung geometries, representative of the respiratory airways of adult Andean women, was 33.0 ± 0.75% of the inhaled mass, with 14.9 ± 0.76% depositing in the intrathoracic airways. The majority of coarse PM mass deposited in the extrathoracic airways, where deposition occurs primarily via impaction [40,41]. On the other hand, most of the fine PM deposited in the intrathoracic airways with 59.7% of this mass reaching the alveolar region, where Browning diffusion is the dominant deposition mechanism. Deposited mass was greatest in the pulmonary region, while tissue dose (DM/TSA) was largest in the lobar and segmental bronchi. The peak in DM between generations 18 and 22 can be attributed to diffusion of PM $\lesssim$ 0.5 μm and sedimentation of PM 1 to 5 μm, while the secondary peak between generations 3 and 5 arises due to impaction of PM $\gtrsim$ 5 μm [42]. Substantial intersubject variability in deposited mass was observed in both the upper bronchial airways and the acinar region. Differences in the upper bronchi are caused by geometric variation, which primarily affects deposition by impaction. On the other hand, differences in the acinar region arise due to variation in the number of alveolated airways, which affects deposition by diffusion and sedimentation, and in the upstream filtering in the tracheobronchial region. Similar results were observed for deposited surface area and DSA/TSA.

Mean daily LDSA concentration was 1009.6 ± 1469.8 $\mu m^2/cm^3$ and mean LDSA during cooking was 10,552.5 ± 8261.6 $\mu m^2/cm^3$. Very few studies have reported LDSA from biomass cookstove emissions, however the concentrations we found are comparable, albeit higher, to data in the literature. De la Sota et al. [33] measured LDSA in 3 households using traditional stoves in rural Senegal and reported a mean LDSA of 5085.9 ± 2980.1 $\mu m^2/cm^3$ during cooking. Another study conducted in rural India found mean LDSA concentrations of 4677.5 ± 8550.7 $\mu m^2/cm^3$ and 6648.6 ± 4845.3 $\mu m^2/cm^3$ during cooking in kitchens with and without a chimney, respectively [43]. Our results add to this limited literature, which could serve as a reference for future studies. The higher LDSA found in our setting could potentially indicate a higher concentration of fine/ultra-fine particles which have particularly detrimental health effects [44,45].

Daily mean DSA doses in the intrathoracic airways were estimated to be 141.6 ± 206.2 cm^2/day, based on the kitchen PSD and personal exposure concentrations. A study on cigarette smoke particles (CSP) conducted in Italy, estimated the intrathoracic particle surface area dose from mainstream cigarette smoke to be 885 cm^2/day for typical adult female smokers [46]. This study reported an average of 11.8 cigarettes per day for female smokers, with an average 11.5 puffs per cigarette and a puff time of 1.8s, resulting in a total puff time of approximately 4 minutes per day. These findings suggest that while exposure to CSP occurs over a shorter daily duration compared to biomass smoke exposure, deposited doses in smokers tend to be higher, on average. Increased time spent in the kitchen during cooking would of course increase lung-deposited doses of biomass PM and could result in comparable deposition to that in smokers. The upper bound estimate of daily intrathoracic deposited dose, based on mean kitchen concentration, is 1479.8 ± 1159.8 cm^2/day. These results highlight the importance of taking into account time spent in the kitchen, if personal exposure measurements are not available.

A number of factors are likely contributors to the lower daily dose from biomass smoke exposure compared to CSP. First, although the PSD of mainstream cigarette smoke (MCS) is similar to that of biomass smoke [47], particle number concentrations of MCS typically range between 10^9 cm^{-3} and 10^{10} cm^{-3} [47-49] compared to average concentrations of approximately 10^3 to 10^5 cm^{-3} during biomass burning, as reported in the current study and others [34]. Second, oral inhalation during smoking results in lower filtration fractions in the extrathoracic airways compared to the nasal route. Finally, higher inhalation flow rates in cigarette puffing compared to regular nasal breathing result in higher deposition via impaction.

Estimated lung-deposited doses in this study were based on the average lung capacity and ventilation characteristics of Andean women. The mean FRC of this population is larger than that of Peruvian women living at sea level [28], and tidal volumes and breathing frequencies also tend to be higher at high altitude. For the same PSD and PM concentrations, we would expect lung-deposited doses to increase with a smaller FRC, although FRC effects on deposition have been found to be small, even with significant volumetric changes [31]. Lower tidal volumes and breathing frequencies would result in lower flow rates, which would decrease deposition via impaction but increase sedimentation and diffusional deposition [50,14]. It is therefore unclear what the overall effect of these changes in lung

capacity and ventilation would be on the total and regional deposited doses at sea level, as deposition is influenced by a complex interplay between lung geometry, ventilation and particle size.

We note that in the present study, daily lung-deposited doses were estimated based on the kitchen PSD, which does not take into account that the PSD of inhaled PM outside the kitchen may differ. However, studies have shown that ambient air pollution in rural Puno is not likely to contribute heavily to the exposures experienced by those cooking with biomass [51], and other indoor PM concentrations (e.g. in the bedroom) are also expected to be low compared to those in the kitchen. Therefore, accounting for the different PSDs and time spent in various micro-environments (e.g. kitchen, outdoors, or bedroom) is not likely to have a major effect on the daily lung-deposited dose estimates.

In addition, particles under 0.3 μm in diameter were not measured and instead were estimated using a nonlinear least-squares optimization method to fit our data with a continuous PSD model. These small particles pose the greatest risk as they can penetrate deep into the lungs and enter the bloodstream, enabling them to diffuse into other organs including the heart, brain and nervous system. Small particles also appear to be cleared less quickly from the lung than larger particles, resulting in greater accumulation in the airway tissue which furthers their interaction with lung cells as well as their translocation beyond the epithelial barrier [52]. However, few studies have measured the ultrafine particles generated from biomass combustion, and epidemiological evidence of their health effects remains relatively scarce [44] and requires further investigation. Despite this limitation, the size-resolved number concentrations above 0.3 μm collected in this study provide a greater resolution compared to $PM_{2.5}$ and PM_{10} typically measured in HAP studies.

Finally, the lung deposition model did not take into account hygroscopic growth, coagulation, particle charge or cloud behavior of the particulate matter within the respiratory tract. Robinson and Yu [48] examined these effects on CSP deposition and found that particle charge, hygroscopic growth and coagulation had a minor effect, whereas tracheobronchial deposition increased when cloud behavior was considered. However, a complete description of cloud behavior in the respiratory airways is currently lacking. For example, the effective cloud diameter is unknown, and was set to an arbitrary value of 2/3 the diameter of the trachea in the study by Robinson and Yu [48]. In addition, the effects of the airway geometry and inter-particle interactions are also unknown. While further work is clearly

required to better understand and model cloud behavior in general, we expect this effect to be smaller in the case of biomass smoke, given that particle concentrations are significantly lower than in fresh MCS. A recent study on the hygroscopic effects of soot particles found that during the first 25 hours of the aerosol aging process, deposition efficiencies from a zero-hygroscopicity simulation were between 0.15% and 0.78% and between 0.5% and 2.4% higher than those of a particle-resolved simulation for the tracheobronchial and alveolar regions, respectively [53]. No significant difference was observed in extrathoracic deposition. Within the first three hours, which is the approximate cooking duration in our sampled households, tracheobronchial and alveolar depositions differed by no more than 1.1% and 0.28%, respectively. Taking into account hygroscopic growth but assuming an average mixing state on the other hand, underestimates deposition in the alveoli by up to 5% for aged soot and 20% for fresh soot [54]. These results suggest that neglecting PM hygroscopicity has a relatively small effect on regional deposition, but further work would be needed to determine its impact at a more granular level.

Despite the limitations discussed above, our study provides a novel approach to determine PM exposure in HAP studies. We present unique data regarding PM deposition in the lungs from exposure to biomass smoke, and demonstrate the use of particle-size measurements and lung deposition models for exposure assessment. The lung-deposited dose provides a more biologically-relevant metric compared to personal exposure alone, and could be used to develop improved dose-response curves. In addition, regional deposition estimates can provide valuable insight into the areas of the lung receiving the highest cumulative doses, which could point to the sites most prone to inflammation and disease initiation. These models can also be a useful tool in helping to understand the pathophysiological differences between biomass-related and cigarette smoke-induced lung damage and disease progression.

References

1. Bruce N, Perez-Padilla R, Albalak R. Indoor air pollution in developing countries: A major environmental and public health challenge. Bull World Health Organ 2000;78:1078–1092.
2. Lim SS, Vos T, Flaxman AD, et al. A comparative risk assessment of burden of disease and injury attributable to 67 risk factors and risk factor clusters in 21 regions, 1990-2010: a systematic analysis for the global burden of disease study 2010. Lancet 2012;380:2224–2260.
3. Fullerton DG, Bruce N, Gordon SB. Indoor air pollution from biomass fuel smoke is a major health concern in the developing world. Trans R Soc of Trop Med Hyg 2008;102:843–851.
4. WHO (World Health Organization), Burden of disease from household air pollution for 2016. https://www.who.int/airpollution/data/HAP_BoD_results_May2018_final.pdf. Accessed 2019-04-29.
5. Martin 2nd WJ, Glass RI, Araj H, et al. Household air pollution in low- and middle-income countries: health risks and research priorities. PLoS Med 2013;10:e1001455.
6. WHO (World Health Organization), WHO air quality guidelines: Global update 2005 (particulate matter, ozone, nitrogen dioxide, and sulfur dioxide); 2006.
7. Park E, Lee K. Particulate exposure and size distribution from wood burning stoves in Costa Rica. Indoor Air 2003;13:253–259.
8. Siddiqui AR, Lee K, Bennett D, et al. Indoor carbon monoxide and $PM_{2.5}$ concentrations by cooking fuels in Pakistan. Indoor Air 2009;19:75–82.
9. Chen C, Zeger S, Breysse P, et al. Estimating indoor $PM_{2.5}$ and CO concentrations in households in southern Nepal: The Nepal cookstove intervention trials. PLoS One 2016;11:e0157984.
10. Jiang R, Bell ML. A comparison of particulate matter from biomass-burning rural and non-biomass-burning urban households in northeastern china. Environ Health Perspect 2008;116:907–914.
11. Armendáriz-Arnez C, Edwards RD, Johnson M, Rosas IA, Espinosa F, Masera OR. Indoor particle size distributions in homes with open fires and improved Patsari cook stoves. Atmos Environ 2010;44:2881–2886.
12. Van Vliet EDS, Asante K, Jack DW, et al. Personal exposures to fine particulate matter and black carbon in households cooking with biomass fuels in rural Ghana. Environ Res 2013;217:40–48.

13. Kleinstreuer C, Zhang Z. Airflow and particle transport in the human respiratory system. Annu Rev Fluid Mech 2010;42:301–334.
14. Nicolaou L. Inertial and gravitational effects on aerosol deposition in the conducting airways. J Aerosol Sci 2018;120:32–5.
15. Hosseini S, Li Q, Cocker D, et al. Particle size distributions from laboratory-scale biomass fires using fast response instruments. Atmos Chem Phys 2010;10:8065–8076.
16. Park SS, Sim SY, Bae MS, Schauer JJ. Size distribution of water-soluble components in particulate matter emitted from biomass burning. Atmos Environ 2013;73:62–72.
17. INEI (Instituto Nacional de Estadistica e Informatica de Peru), Censos nacionales 2017: XII de población, VII de vivienda y III de comunidades indígenas – Resultados definitivos del departamento de Puno (2018). https://www.inei.gob.pe/media/MenuRecursivo/publicaciones_digitales/Est/Lib1563/.
18. Fandiño-Del-Rio M, Goodman D, Kephart JL, et al. Effects of a liquefied petroleum gas stove intervention on pollutant exposure and adult cardiopulmonary outcomes (CHAP): Study protocol for a randomized controlled trial. Trials 2017;18:518.
19. Anjilvel S, Asgharian B. A multiple-path model of particle deposition in the rat lung. Fund Appl Toxicol 1995;28:41–50.
20. Asgharian B, Hofmann W, Bergmann R. Particle deposition in a multiple-path model of the human lung. Aerosol Sci Tech 2001:34:332–339.
21. Raabe OG, Yeh HC, Schum GM, Phalen RF. Tracheobronchial geometry: human, dog, rat, hamster – A compilation of selected data from the project respiratory tract deposition models, Report LF-53. Lovelace Foundation, Albuquerque, New Mexico; 1976.
22. Koblinger L, Hofmann W. Analysis of human lung morphometric data for stochastic aerosol deposition calculations. Phys Med Biol 1985;30:541−556.
23. Grgic B, Finlay W, Burnell P, Heenan A. In vitro intersubject and intrasubject deposition measurements in realistic mouth-throat geometries. J Aerosol Sci 2004;35**:**1025–1040.
24. Heenan A, Finlay W, Grgic B, Pollard A, Burnell P. An investigation of the relationship between the flow field and regional deposition in realistic extra-thoracic airways. J Aerosol Sci 2004;35:1013–1023.

25. Nicolaou L, Zaki TA. Direct numerical simulations of flow in realistic mouth-throat geometries. J Aerosol Sci 2013;57:71–87.
26. Koullapis P, Nicolaou L, Kassinos SC. In silico assessment of mouth-throat effects on regional deposition in the upper tracheobronchial airways. J Aerosol Sci 2018;117:164–188.
27. Yeh HC, Schum GM. Models of human lung airways and their application to inhaled particle deposition. Bull Math Biol 1980;42:461–480.
28. McAuliffe F, Kametas N, Espinoza J, Greenough A, Nicolaides K. Respiratory function in pregnancy at sea level and at high altitude. BJOG 2004;111:311–315.
29. ICRP (International Commission on Radiological Protection), Human respiratory tract model for radiological protection. ICRP Publication 66. Ann ICRP 24(1–3); 1994.
30. Beall CM, Strohl KP, Blangero J, et al. Ventilation and hypoxic ventilatory response of Tibetan and Aymara high altitude natives. Am J Phys Anthropol 1997;104:427–447.
31. Hofmann W, Asgharian B, Winkler-Heil R. Modeling intersubject variability of particle deposition in human lungs. J Aerosol Sci 2002;**33**:219–235.
32. Kuula J, Kuuluvainen H, Niemi JV, et al. Long-term sensor measurements of lung deposited surface area of particulate matter emitted from local vehicular and residential wood combustion sources. Aerosol Sci Tech 2019;54(2):190–202.
33. de la Sota C, Lumbreras J, Pérez N, Ealo M, Kane M, Youm I, Viana M. Indoor air pollution from biomass cookstoves in rural Senegal. Energy Sustain Dev 2018;43:224–234.
34. Reid JS, Koppmann R, Eck TF, Eleuterio DP. A review of biomass burning emissions Part II: Intensive physical properties of biomass burning particles. Atmos Chem Phys 2005;5:799–825.
35. Janhäll S, Andreæ MO, Pöschl U. Biomass burning aerosol emissions from vegetation fires: particle number and mass emission factors and size distributions. Atmosph Chem Phys 2010;10:1427–1439.
36. Brauer M, Bartlett K, Regalado-Pineda J. Assessment of particulate concentrations from domestic biomass combustion in rural Mexico. Environ Sci Technol 1995;30(1):104–109.
37. Naeher LP, Smith KR, Leaderer BP, Mage D, Grajeda R. Indoor and outdoor $PM_{2.5}$ and CO in high-and low-density Guatemalan villages. J Expo Sci Environ Epidemiol 2000;10(6):544–51.

38. Ni K, Carter E, Schauer JJ, Ezzati M, Zhang Y, Niu H, Lai AM, Shan M, Wang Y, Yang X, Baumgartner J. Seasonal variation in outdoor, indoor, and personal air pollution exposures of women using wood stoves in the Tibetan Plateau: Baseline assessment for an energy intervention study. Environ Int 2016;94:449–57.
39. Albalak R, Keeler GJ, Frisancho AR, Haber M. Assessment of PM_{10} concentrations from domestic biomass fuel combustion in two rural Bolivian highland villages. Environ Sci Technol 1999;33(15):2505–9.
40. Koullapis P, Kassinos SC, Muela J, et al. Regional aerosol deposition in the human airways: The Siminhale benchmark case and a critical assessment of *in silico* methods. Eur J Pharm Sci 2018;113:77–94.
41. Nicolaou L, Zaki TA. Characterization of aerosol Stokes number in 90° bends and idealized extrathoracic airways. J Aerosol Sci 2016;102:105–127.
42. Deng Q, Deng L, Miao Y, Guo X, Li Y. Particle deposition in the human lung: health implications of particulate matter from different sources. Environ Res 2019;169:237–45.
43. Patel S, Leavey A, Sheshadri A, Kumar P, Kandikuppa S, Tarsi J, Mukhopadhyay K, Johnson P, Balakrishnan K, Schechtman KB, Castro M. Associations between household air pollution and reduced lung function in women and children in rural southern India. J Appl Toxicol 2018;38(11):1405–15.
44. Ohlwein S, Kappeler R, Kutlar Joss M, Künzli N, Hoffmann B. Health effects of ultrafine particles: a systematic literature review update of epidemiological evidence. Int J Public Health 2019;64:547–559.
45. Ibald-Mulli A, Wichmann HE, Kreyling W, Peters A. Epidemiological evidence on health effects of ultrafine particles. J Aerosol Med 2002;15(2):189-201.
46. Fuoco FC, Stabile L, Buonanno G, Scungio M, Manigrasso M, Frattolillo A. Tracheobronchial and alveolar particle surface area doses in smokers. Atmosphere 2017;8:19.
47. Chang PT, Peters LK, Ueno Y. Particle size distribution of mainstream cigarette smoke undergoing dilution. Aerosol Sci Tech 1985;4:191–207.
48. Robinson RJ, Yu CP. Deposition of cigarette smoke particles in the human respiratory tract. Aerosol Sci Tech 2001;34:202–215.

49. Alderman SL, Ingebrethsen BJ. Characterization of mainstream cigarette smoke particle size distributions from commercial cigarettes using a DMS500 fast particulate spectrometer and smoking cycle simulator. Aerosol Sci Tech 2011;45:1409–1421.
50. Phalen RF, Oldham MJ, Beaucage CB, Crocker TT, Mortensen J. Postnatal enlargement of human tracheo-bronchial airways and implications for particle deposition. Anat Rec 1985;212:368–380.
51. Pollard SL, Williams DL, Breysse PN, et al. CRONICAS Cohort Study Group, A cross-sectional study of determinants of indoor environmental exposures in households with and without chronic exposure to biomass fuel smoke. Environ Health 2014;13:21.
52. Health Effects Institute, Understanding the health effects of ambient ultrafine particles. HEI Perspectives 3 2013. https://www.healtheffects.org/system/files/Perspectives3.pdf.
53. Ching J, Kajino M. Aerosol mixing state matters for particles deposition in human respiratory system. Sci Rep 2018;8(1):1–11.
54. Stevens R, Dastoor A. A Review of the Representation of Aerosol Mixing State in Atmospheric Models. Atmosphere 2019;10(4):168.

Appendix

Cardiopulmonary outcomes and Household Air Pollution (CHAP) trial Investigators: Steering Committee: William Checkley MD PhD (Johns Hopkins University, Baltimore, MD, USA), Gustavo F Gonzales MD (Universidad Peruana Cayetano Heredia, Lima, Peru), Luke Naeher PhD (University of Georgia, Athens, GA, USA), Joshua Rosenthal PhD (National Institutes of Health, Bethesda, MD, USA), N Kyle Steenland PhD (Emory University, Atlanta, Georgia, USA). Johns Hopkins University Investigators: Theresa Aguilar, Vanessa Burrowes PhD, Magdalena Fandiño-Del-Rio MSc, Elizabeth C Fung MSPH, Dina Goodman MSPH, Steven A Harvey PhD, Phabiola Herrera MD, Josiah L Kephart PhD, Kirsten Koehler PhD, Alexander Lee, Kathryn A Lee MPH, Catherine H Miele MD MPH, Mitra Moazzami MSPH, Lawrence Moulton PhD, Saachi Nangia, Laura Nicolaou PhD, Carolyn O'Brien MSPH, Suzanne Simkovich MD MS, Timothy Shade, Lena Stashko MSPH, Ariadne Villegas-Gomez MSPH, Kendra N Williams PhD, Abigail Winiker MSPH. Asociación Benéfica PRISMA Investigators: Marilu Chiang MD MPH, Gary Malpartida, Carla Tarazona-Meza MPH. Washington University Investigators: Victor Davila-Roman MD, Lisa de las Fuentes MD. Emory

University Investigators: Dana Barr Boyd PhD, Maria Jolly MSPH, Angela Rozo. RTI International: Ryan Chartier, PhD.

Table 1. Estimated daily deposited doses of PM from biomass smoke based on personal exposures.

Deposited dose		Mass (μg/day)		Surface area (cm^2/day)	
		mean ± SD	median (IQR)	mean ± SD	median (IQR)
Regional	ETA	411.7 ± 598.8	257.8 (140.7 – 465.8)	31.4 ± 45.7	19.7 (10.8 – 21.8)
	TB	137.8 ± 200.5	85.9 (47.6 – 156.7)	57.7 ± 83.9	35.8 (19.9 – 65.8)
	Pulm	201.3 ± 294.3	124.5 (69.2 – 229.4)	83.9 ± 122.7	51.9 (28.9 – 95.7)
	Total	**750.8 ± 1092.2**	**470.3 (259.3 – 855.0)**	**173.0 ± 251.9**	**107.0 (60.3 – 197.2)**
Lobar	LU	55.8 ± 85.4	33.2 (18.4 – 62.7)	23.2 ± 35.5	13.8 (7.7 – 26.1)
	LL	85.7 ± 133.7	51.0 (27.8 – 95.7)	35.8 ± 55.8	21.2 (11.6 – 39.9)
	RU	76.9 ± 127.3	44.0 (23.3 – 83.8)	32.0 ± 53.0	18.4 (9.7 – 35.1)
	RM	33.2 ± 60.1	17.7 (8.8 – 35.6)	13.8 ± 25.0	7.3 (3.7 – 14.8)
	RL	60.4 ± 99.6	34.3 (17.1 – 68.2)	25.2 ± 41.5	14.3 (7.1 – 28.4)

Figure legends

Figure 1. Personal exposures and kitchen concentrations of $PM_{2.5}$ as obtained from the 48-hour time-weighted gravimetric measurements: (a) probability densities; (b) box plots. Mean personal exposure concentration and kitchen area concentration denoted by μ_P and μ_K, respectively.

Figure 2. PM number concentrations throughout the day averaged in two-hour intervals for each kitchen.

Figure 3. Mean daily particle size distributions: (a) number-weighted mean and standard deviations; (b) mass-weighted mean and standard deviations. Continuous particle size distribution model plotted in (b). The geometric mean diameters of the accumulation and coarse modes are denoted by d_{ga} and d_{gc}, respectively.

Figure 4. Daily variation of PM in 10-minute intervals: (a) gravimetric-corrected mass concentrations; (b) mass fractions. Mean values were computed across all available one-minute samples at a given time of the day, and then time-averaged in 10-minute intervals.

Figure 5. Fraction of inhaled mass depositing in the lungs. (a) Total and regional deposition fractions in the extrathoracic (ETA), tracheobronchial (TB) and pulmonary airways. (b) Deposition fractions in the left upper (LU), left lower (LL), right upper (RU), right middle (RM), and right lower (RL) lobes. Accumulation and coarse mode PM shown in blue and orange, respectively. Individual lung geometries shown by scatter plot.

Figure 6. Deposition per airway generation over one breathing cycle: (a) Deposited mass (DM), (b) Deposited mass per tissue surface area (DM/TSA), (c) Deposited surface area (DSA), (d) Deposited surface area per tissue surface area (DSA/TSA). Plots show mean ± standard deviation of the total deposition in a given generation, mean deposition of the accumulation and coarse mode particles, and deposition in each of the individual lung geometries.

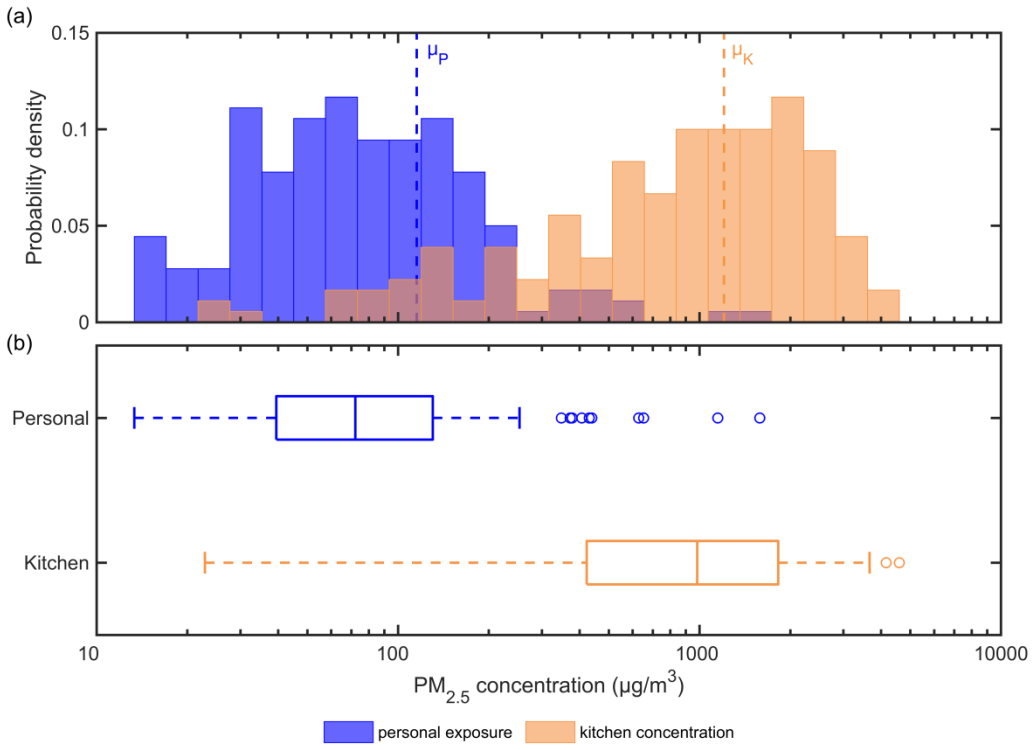

ina_12710_f1.tiff

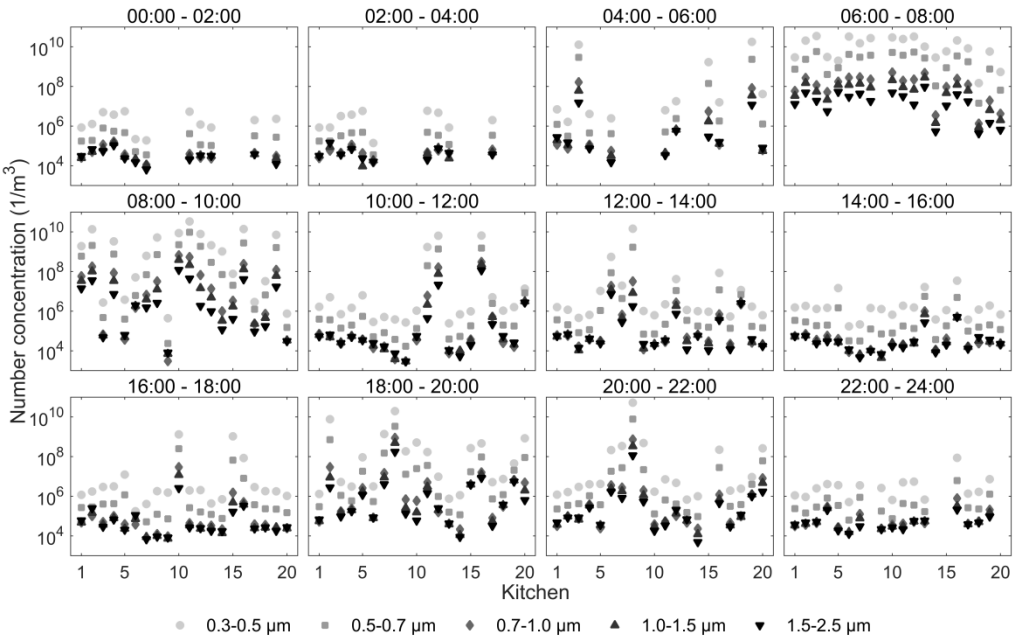

ina_12710_f2.tiff

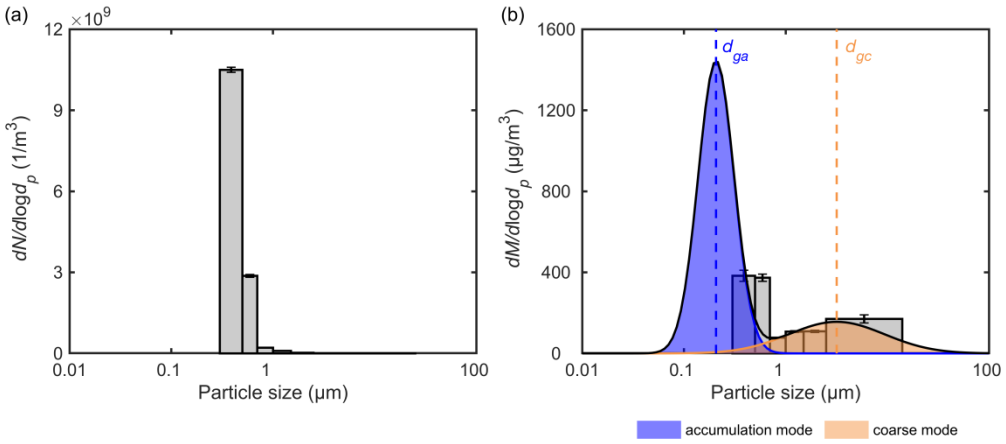

ina_12710_f3.tiff

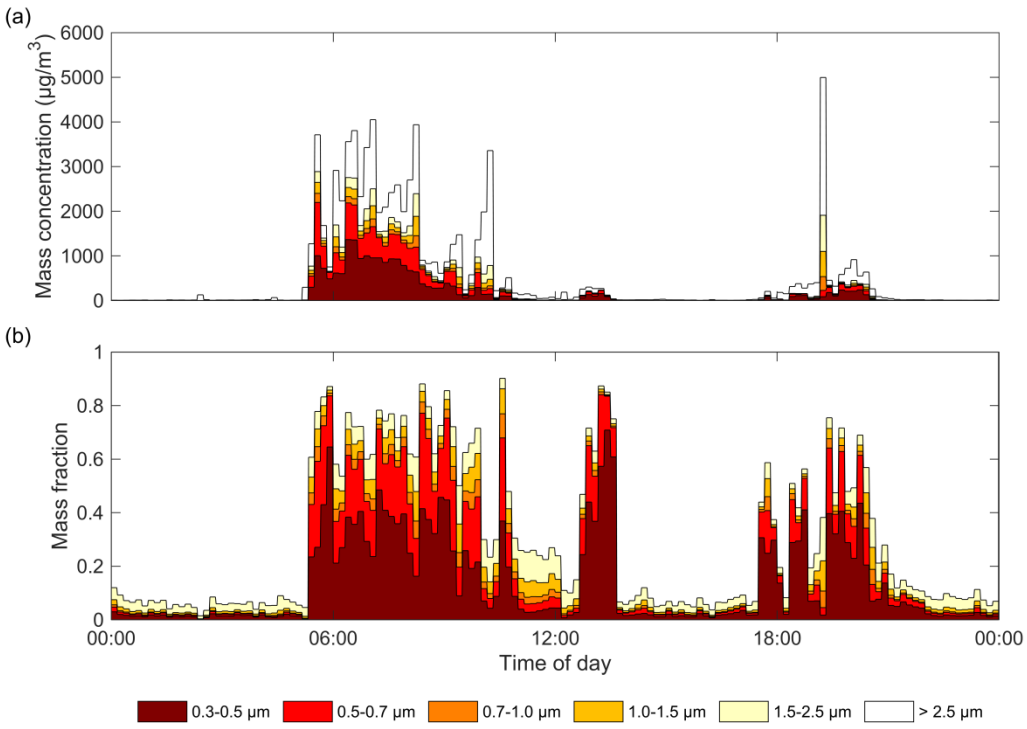

ina_12710_f4.tiff

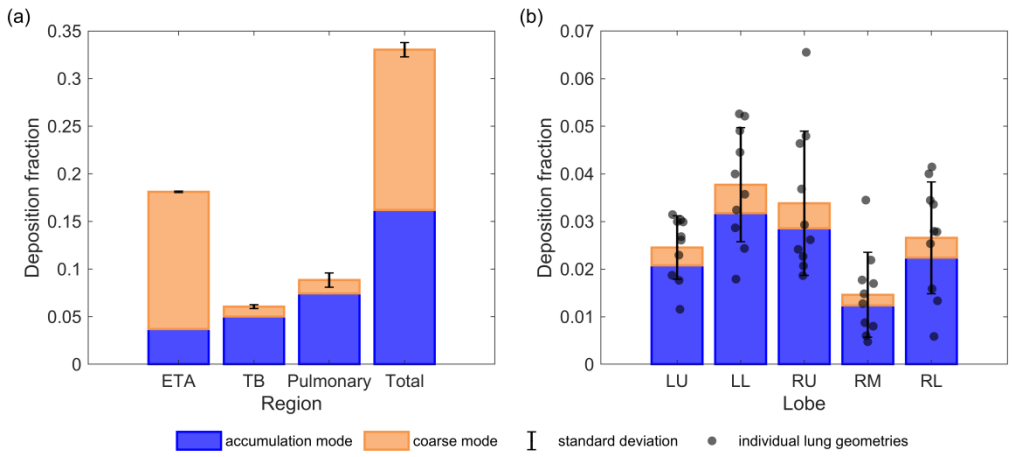

ina_12710_f5.tiff

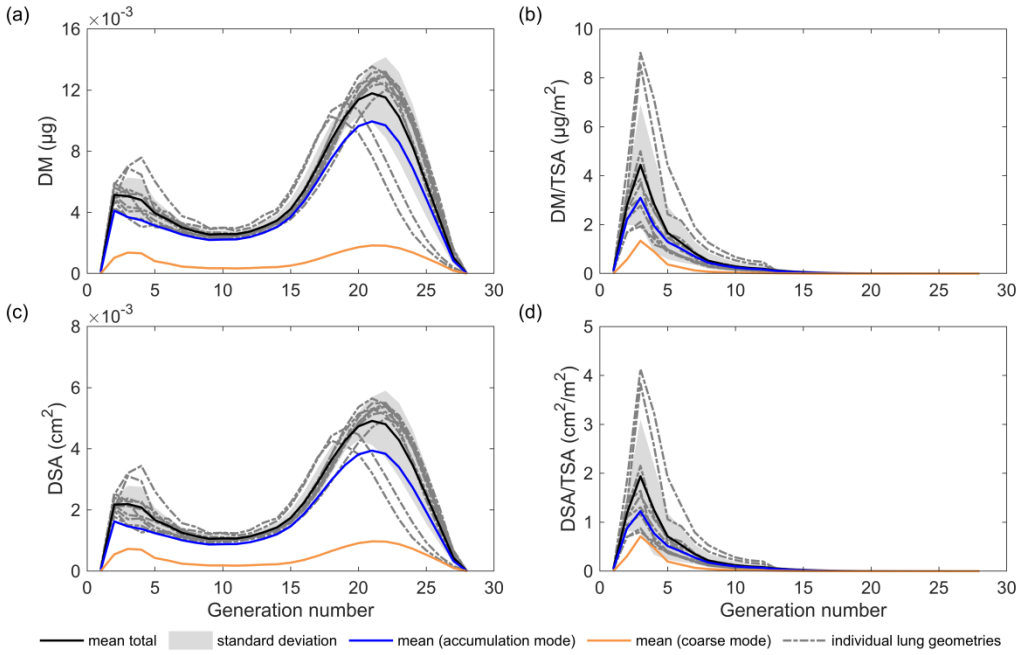

ina_12710_f6.tiff